NANO · MICRO small
www.small-journal.com

Lattice Strained B-Doped Ni Nanoparticles for Efficient Electrochemical H_2O_2 Synthesis

Hui Fu, Nan Zhang, Feili Lai, Longsheng Zhang, Zhenzhong Wu, Hanjun Li, Haiyan Zhu, and Tianxi Liu**

Surface strains are necessary to optimize the oxygen adsorption energy during the oxygen reduction reaction (ORR) in the four-electron process, but the surface strains regulation for ORR in the two-electron process to produce hydrogen peroxide (H_2O_2) is rarely studied. Herein, it is reported that the tensile strained B-doped Ni nanoparticles on carbon support (Ni-B@BNC) could enhance the adsorption of O_2, stabilize O—O bond, and boost the electrocatalytic ORR to H_2O_2. Moreover, the Ni-B@BNC catalysts exhibit volcano-type activity for electrocatalytic ORR to H_2O_2 as a function of the strain intensity, which is controlled by B content. Among them, Ni_4-B_1@BNC exhibits the highest H_2O_2 selectivity of over 86%, H_2O_2 yield of 128.5 mmol h^{-1} g^{-1}, and Faraday efficiency of 94.9% at 0.6 V vs reversible hydrogen electrode as well as durable stability after successive cycling, being one of the state-of-the-art electrocatalysts for two-electron ORR. The density functional theory calculations reveal that tensile strain introduced by doping B into Ni nanoparticles could decrease the state density of Ni-3d orbital and optimize the binding energy of OOH* during ORR. A new direction is provided here for the design of highly active and stable catalysts for potential H_2O_2 production and beyond.

1. Introduction

Hydrogen peroxide (H_2O_2), the versatile and environmentally friendly oxidant, is significant for various industries including wastewater treatment, chemical synthesis, pulp and textile bleaching, potential energy carrier, and disinfectants, etc.[1–5] Due to its wide application, the demand for H_2O_2 is increasing rapidly. In industry, anthraquinone process is the most widely used technique for large-scale H_2O_2 synthesis.[6,7] Nevertheless, it is a multistep method consisting of sequential hydrogenation and oxidation steps in an organic solvent followed by extraction and further distillation, which involves energy-intensive distillation, hazardous wastes, and unstable bulk H_2O_2 solutions.[2] One alternative route is the direct synthesis from H_2 and O_2 to produce H_2O_2.[8] However, high purity H_2 and O_2 need to be diluted with inert carrier gas (N_2 or CO_2) to prevent explosion, resulting in low selectivity and production rate toward H_2O_2. Therefore, it is of significance to seek a green, effective, and safe route for H_2O_2 synthesis.

Electrocatalytic oxygen reduction reaction (ORR) provides an attractive route for the production of H_2O_2, as it can effectively address the unsafe and nongreen problems of anthraquinone method and direct synthesis.[9–12] But the sluggish kinetics and competing reaction of four-electron pathway in ORR seriously affect the efficiency and yield of H_2O_2.[13–15] The correlation studies indicate that the optimization of O_2 adsorption energy and preservation of the O—O bond are key to generate H_2O_2 efficiently.[16,17] Earth-boundant transition metal such as Ni has shown great promises for the two-electron ORR, and numerous studies linking to the modification, defection, and composition upon optimizing the natural properties of transition metal and tailoring their two-electron ORR activities have gained momentum.[18–20] Among them, strain engineering generated by the lattice mismatch with the different structure or components has been necessary to optimize the oxygen adsorption energy during the electrocatalytic four-electron ORR, but is rarely reported for two-electron ORR.

Herein, we synthesized a new class of B-doped Ni nanoparticles supported on B/N codoped carbon (Ni-B@BNC) composites with tensile strain as an active and stable catalyst for electrocatalytic ORR to generate H_2O_2 in alkaline solution. In detail, the tensile strained Ni-B@BNC composites exhibit volcano-type activity for electrocatalytic ORR to H_2O_2 as a function of strain intensity, which is controlled by B content Ni_4-B_1@BNC exhibits a high H_2O_2 selectivity of over 86%, H_2O_2 yield of 128.5 mmol h^{-1} g^{-1} and FE_{H2O2} of 94.9% at 0.6 V_{RHE}, respectively. In addition, the N_4-B_1@BNC can stably generate H_2O_2 for 10 h at 0.4 V_{RHE} in 0.1 M KOH. The high H_2O_2 selectivity can also be maintained even after five cycles. The density functional theory (DFT) calculations indicate that tensile strain introduced by doping B into Ni nanoparticles could decrease

H. Fu, N. Zhang, L. Zhang, Z. Wu, H. Li, H. Zhu, T. Liu
The Key Laboratory of Synthetic and Biological Colloids
Ministry of Education
School of Chemical and Material Engineering
International Joint Research Laboratory for Nano Energy Composites
Jiangnan University
Wuxi 214122, China
E-mail: nzhang@jiangnan.edu.cn; txliu@jiangnan.edu.cn
F. Lai
Department of Chemistry
KU Leuven
Celestijnenlaan 200F, Leuven 3001, Belgium
The ORCID identification number(s) for the author(s) of this article can be found under https://doi.org/10.1002/smll.202203510.

DOI: 10.1002/smll.202203510

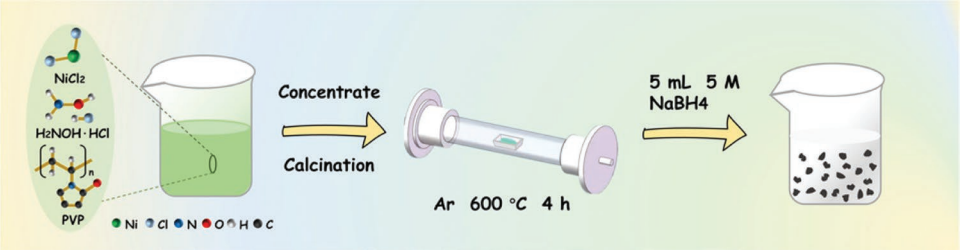

Scheme 1. Schematic illustration of the preparation of Ni_4-B_1@BNC.

the state density of Ni-3d orbital near the Fermi level and optimize the binding energy of OOH* for two-electron ORR.

2. Results and Discussion

As shown in **Scheme 1**, Ni_4-B_1@BNC composites were synthesized boronation with sodium borohydride ($NaBH_4$) as boron source (see Experimental procedures in the Supporting Information for detail). Furthermore, the Ni@NC sample obtained without boronation process were prepared as a comparison (**Figure 1**a,b). As shown in Figure 1c and Figure S1 in the Supporting Information, the surface of Ni_4-B_1@BNC becomes rougher than before boronization. In addition, the Ni@NC with porous structure is observed. The scanning electron microscopy energy-dispersive X-ray spectroscopy (SEM-EDS) spectra (Figure S2a, Supporting Information) further reflect that the atomic ratio of Ni and B is closed to 4:1 when the feed ratio of

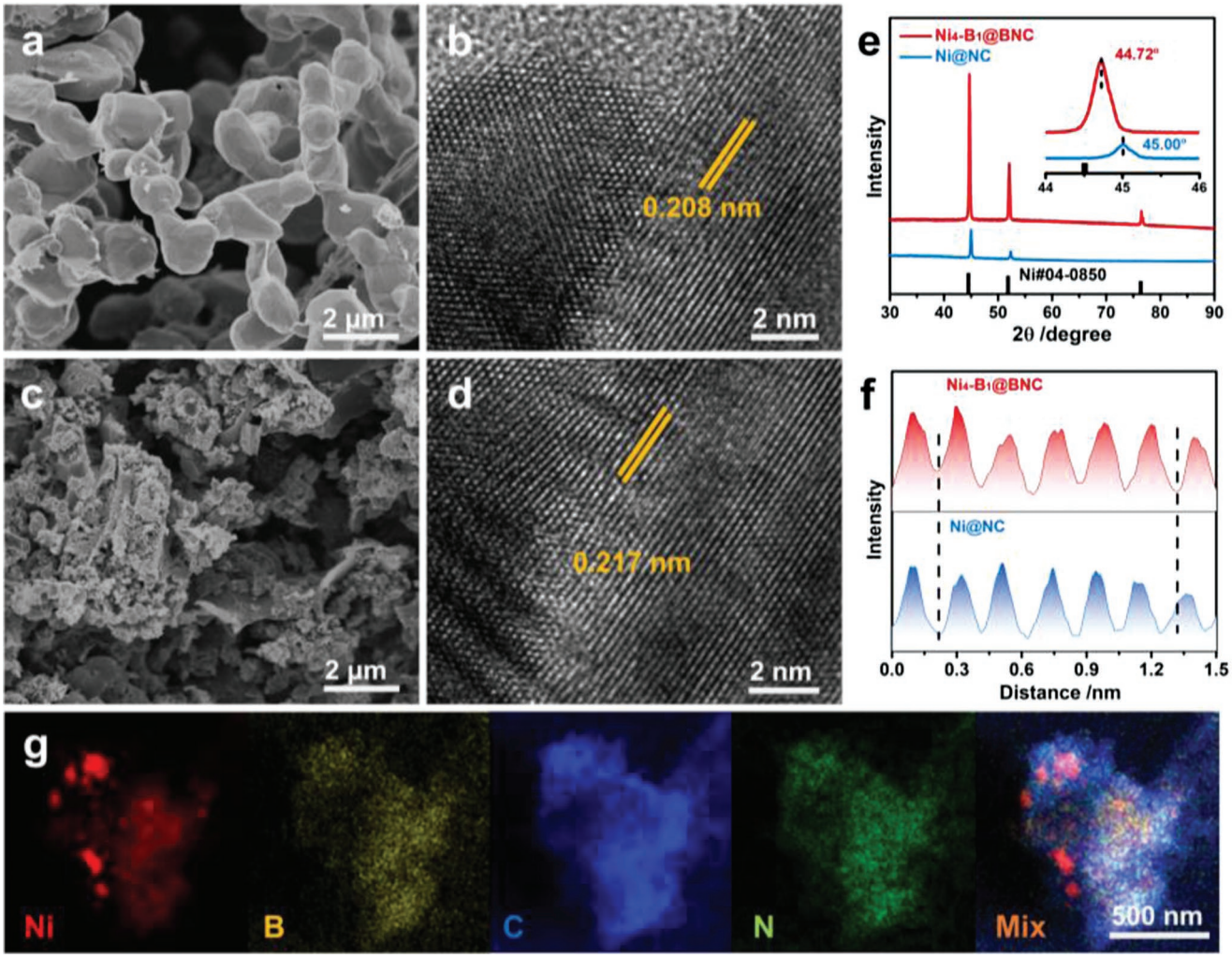

Figure 1. Structural and compositional characterizations of catalysts. a) SEM image and b) HRTEM image of Ni@NC. c) SEM image and d) HRTEM image of Ni_4-B_1@BNC. e) PXRD patterns of Ni@NC and Ni_4-B_1@BNC. f) Integrated pixel intensities of Ni {111} lattices of Ni_4-B_1@BNC and Ni@NC. g) TEM-EDS elemental mappings of Ni_4-B_1@BNC.

Ni and B is 1:3. As further revealed by X-ray photoelectron spectroscopy (XPS), two elements N and B have been successfully doped into the sample (Figure S2b–d, Supporting Information). Moreover, the lattice spacing of Ni@NC is 0.208 nm on the basis of high-resolution transmission electron microscopy (HRTEM) image, which corresponds to the {111} facet of Ni (Figure 1b). As for Ni_4-B_1@BNC (Figure 1d), the lattice spacing 0.217 nm is larger than that of Ni@NC, which is in line with the powder X-ray diffraction (PXRD) results that the diffraction peaks of Ni_4-B_1@BNC at {111} facet shift to a lower angle than that of Ni@NC, suggesting the doping B atoms induces a lattice expansion in Ni crystals (Figure 1e).[21–23] Moreover, the pixel intensities of the Ni {111} facet selected from the HRTEM images of Ni_4-B_1@BNC and Ni@NC are shown in Figure 1f. Due to the introduction of B, Ni_4-B_1@BNC exhibits a typical tensile strain compared with Ni@NC. The elemental mappings were also conducted to reveal the element distribution on the Ni_4-B_1@BNC. It is obvious that Ni, B, N, and C evenly distributed over Ni_4-B_1@BNC (Figure 1g and Figure S2e, Supporting Information), further indicating that B and N have been codoped successfully. In a word, the results above indicate that B induces tensile strain in Ni@NC.

As shown in **Figure 2**, the ORR properties of Ni-B@BNC were investigated and compared with Ni@NC and BNC (Figure S3, Supporting Information). Before electrochemical measurement, the reference electrode potentials were calibrated in 0.1 M KOH (Figure S4, Supporting Information).[24] The electrochemical active surface area (ECSA) of the different catalysts were measured by the double-layer capacitance (C_{dl}) values in 0.1 M KOH.[25] As displayed in Figure S5 in the Supporting Information, the C_{dl} of Ni_4-B_1@BNC is 1.84 mF cm^{-2}, which is higher than those of the Ni@NC (0.42 mF cm^{-2}) and BNC (1.32 mF cm^{-2}). The larger ECSA of Ni_4-B_1@BNC is beneficial for exposing more active sites to enhance the electroreduction activity. The ORR properties of the three different catalysts were tested with a rotating ring disk electrode (RRDE) setup at 1600 rpm in O_2-saturated 0.1 M KOH. The voltage on the ring electrode of Pt is set to 1.2 V_{RHE}, which can be used to collect and quantify the H_2O_2. The value of collection efficiency (N) was experimentally determined to be 0.36 by using a standard ferricyanide system (Figure S6, Supporting Information). The O_2 reduction disk currents and the measured peroxide oxidation ring currents for Ni_4-Bi_1@BNC, Ni@NC, and BNC were shown in Figure 2a. By calculating the ring and disk current, it can be found that Ni_4-B_1@BNC exhibits the highest H_2O_2 selectivity of 86% among the three different catalysts in the range of 0.2_0.6–V_{RHE}, which is much higher than those of the BNC (51%) and Ni@NC (35%) (Figure 2b), revealing that the tensile strained Ni_4-B_1@BNC could optimize the maintenance of O—O bond during ORR. Simultaneously, as shown in Figure 2c, the number of transferred electrons (n) of the Ni_4-B_1@BNC during ORR is estimated to be around 2.0, further suggesting a dominant two-electron O_2 reduction pathway of N_4-B_1@BNC. In addition, the rotating-disk voltammetry experiments were carried out at different rotating speeds to further verify the ORR catalytic pathway of Ni_4-B_1@BNC (Figure S7a, Supporting Information). The corresponding Koutecky-Levich plots at different potentials are approximately linearity and near parallelism (Figure S7b, Supporting Information), suggesting the first-order reaction kinetic with respect to the concentration of dissolved oxygen and similar electron transfer number for ORR at different potentials. The n was calculated to be about 2.0 of Ni_4-B_1@BNC is dominated by a two-electron oxygen reduction process. Furthermore, the Ni_4-B_1@BNC is also durable since both the ring and disk currents can maintain over 10 h by the potentiostatic measurement (Figure 2d). It is worth noting that the H_2O_2 selectivity and n of N_4-B_1@BNC could remain unchanged after five cycles (Figure 2e). After the durability test, the N_4-B_1@BNC could largely maintain their morphology, valence, and distribution of elements, showing the excellent durability during ORR (Figures S8 and S9, Supporting Information).

Furthermore, the productivity of H_2O_2 was measured in H-cell separated by a proton exchanged membrane (Nafion 117) at room temperature and atmospheric pressure. The potentiostatic tests were conducted in O_2-saturated 0.1 M KOH at different potentials for 2 h (Figure S10, Supporting Information). Then the H_2O_2 produced by the catalysts was quantified with the UV–vis spectroscopy method (Figure S11, Supporting Information). As shown in **Figure 3**a, among the three different catalysts, the Ni_4-B_1@BNC exhibits the highest H_2O_2 yield of 128.5 mmol h^{-1} g^{-1}, nearly 2.4 and 1.6 times higher than those of Ni@NC (52.6 mmol h^{-1} g^{-1}) and BNC (80.2 mmol h^{-1} g^{-1}). The turnover frequency (TOF) of H_2O_2 was calculated to evaluate their intrinsic activity of per active site. TOF of H_2O_2 by Ni_4-B_1@BNC in 2 h reached up to 36.71 h^{-1}, nearly four times higher than that Ni@NC (9.48 h^{-1}). To further evaluate the catalytic activity of catalysts, the Faraday efficiency (FE) of H_2O_2 was also calculated, the FE_{H2O2} of Ni_4-B_1@BNC is as high as 94.9% at 0.6 V_{RHE}, which is much higher than those of Ni@NC (18.1%) and BNC (58.9%) (Figure 3b), indicating a markedly improved catalytic activities toward two-electron ORR of Ni_4-B_1@BNC. Moreover, the H_2O_2 yield and FE_{H2O2} of Ni_4-B_1@BNC for ORR are superior to most electrocatalysts reported (Figure 3c,d), further verifying the important role of tensile strained Ni_4-B_1@BNC in effectively adsorbing O_2 and protecting the O—O bond during ORR. Then, ORR over Ni_4-B_1@BNC was further tested in a flow-cell system to study the potential application in industry (Figure S12a, Supporting Information). We first deposited the catalysts by spray coating a configure ink onto a carbon gas diffusion electrode and the details are given in the Supporting Information. Afterward, ORR performance was evaluated at 0.4 V_{RHE} in 1 M KOH via a potentiostatic test for 4 h (Figure S12b, Supporting Information). In the flow-cell system, the Ni_4-B_1@BNC exhibits the high H_2O_2 yield of 245.5 mmol h^{-1} g^{-1} and excellent durability during ORR.

Furthermore, a series of Ni-B@BNC catalysts with different compositions of Ni and B were prepared to investigate the effect of strain intensity on the catalytic performance. As shown in Figure S13 in the Supporting Information, the structures of the materials are almost the same as the Ni_4-B_1@BNC. The atomic ratio of Ni and B of the two different catalysts were determined to 1:2 and 7:1 by SEM-EDS, and the two different catalysts were named as Ni_1-B_2@BNC and Ni_7-B_1@BNC (Figure S14, Supporting Information). It is worth noting that the more B content, the lower angle the PXRD diffraction peak shifts, indicating that the surface lattice spacing increases with the increase of B content, further revealing that the tensile strain

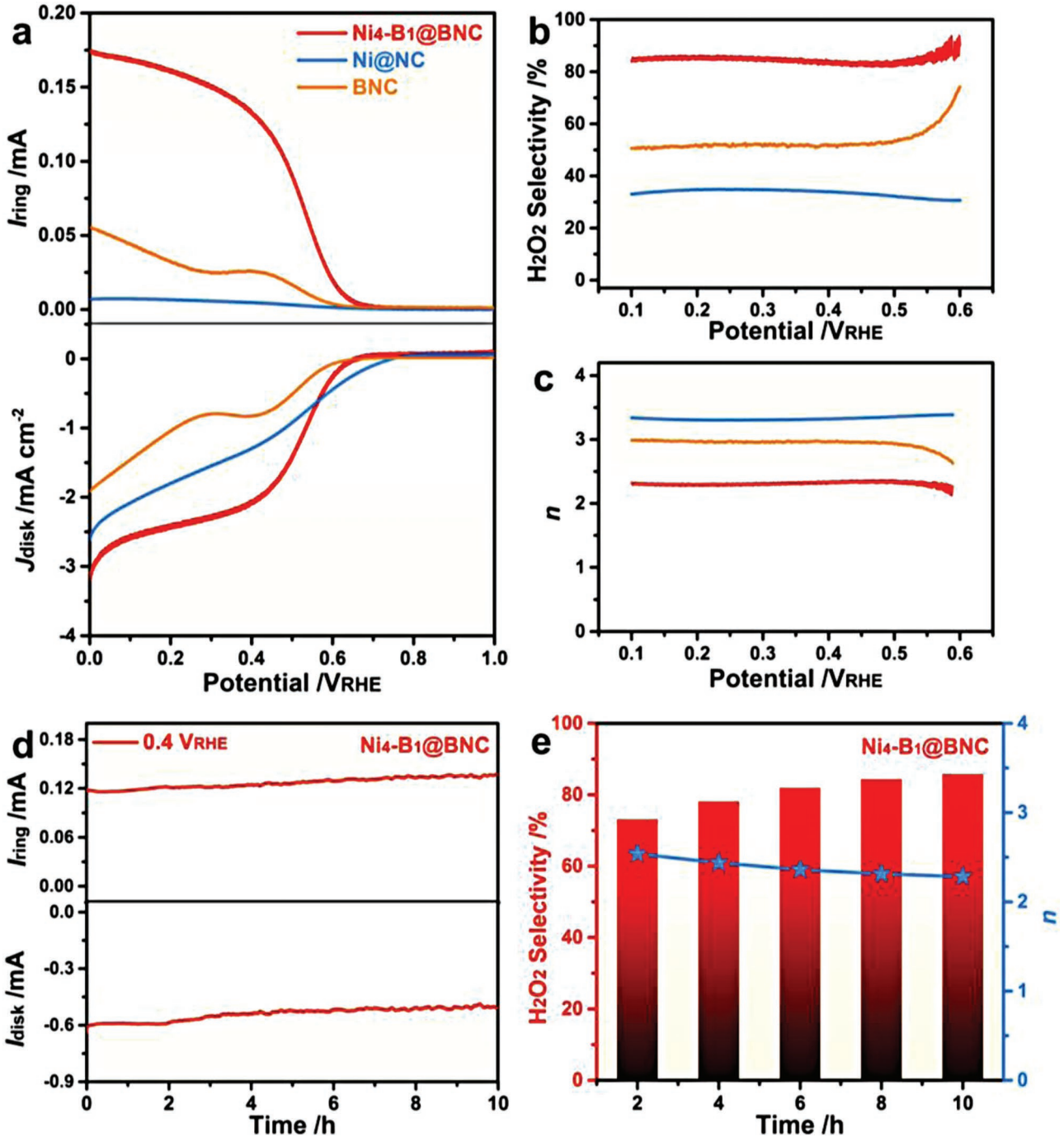

Figure 2. a) RRDE voltammograms of the activated Ni_4-B_1@BNC, Ni@NC, and BNC at 1600 rpm in O_2-saturated 0.1 M KOH with the disk current density and ring current. The scan rate is 10 mV s^{-1}. b) H_2O_2 selectivity as a function of the applied potential. c) The calculated values of n as a function of the applied potential. d,e) 10 h durability test for the activated Ni_4-B_1@BNC at 0.4 V_{RHE} for disk and 1.2 V_{RHE} for ring, and the corresponding H_2O_2 selectivity and *n* in the stabilization process at 2 h intervals.

intensity would be adjusted by changing B content (Figure S15a,b, Supporting Information).[23] In addition, the B 1s and N 1s XPS spectra presented in Figure S15c–e in the Supporting Information. indicate that B and N have been successfully doped into N_1-B_2@BNC and Ni_7-B_1@BNC. As displayed in Figure S16 in the Supporting Information, the C_{dl} of Ni_1-B_2@BNC and Ni_7-B_1@BNC is 1.10 and 1.56 mF cm^{-2}, which are both lower than that of Ni_4-B_1@BNC. The electrochemical ORR properties of Ni_1-B_2@BNC and Ni_7-B_1@BNC were investigated under the same test conditions as Ni_4-B_1@BNC. As shown in Figure S17 in the Supporting Information, Ni_1-B_2@BNC and Ni_7-B_1@BNC show only 63% and 78% of H_2O_2 selectivity, respectively, in the range from 0.2 to 0.6 V_{RHE}. In addition, the corresponding n of the two different catalysts were estimated

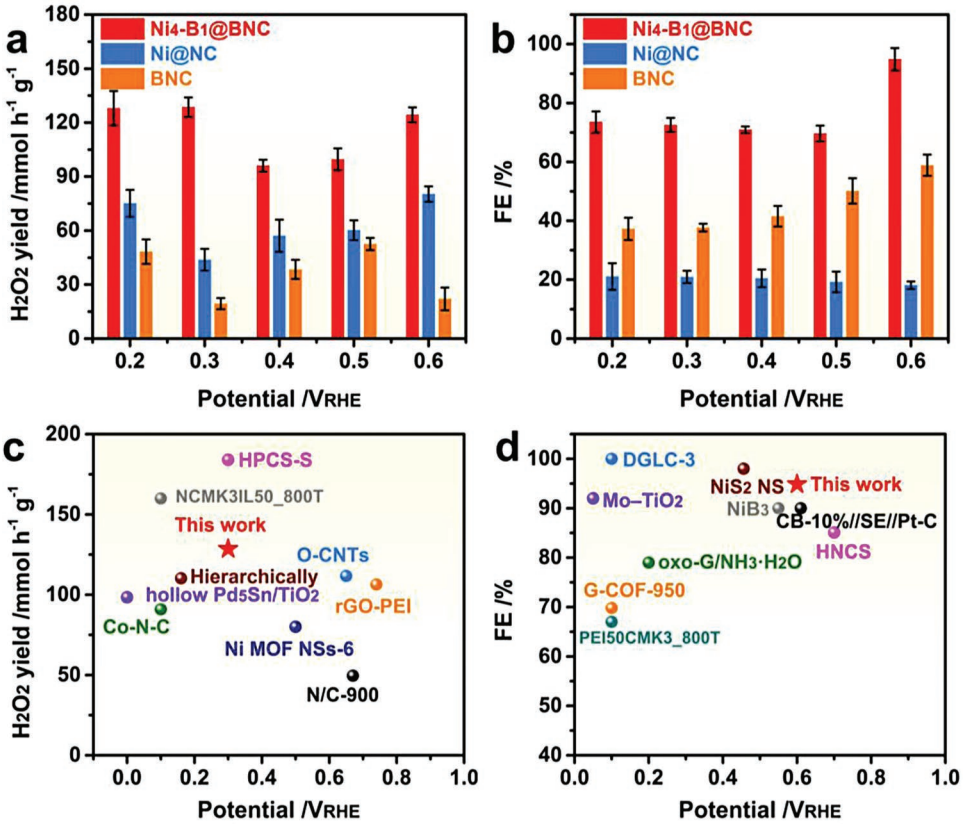

Figure 3. a) H_2O_2 yield and b) FE_{H2O2} of Ni_4-B_1@BNC, Ni@NC, and BNC. Comparison of the c) H_2O_2 yield and d) FE_{H2O2} of Ni_4-B_1@BNC and ORR electrocatalysts reported.

to be around 2.8 and 2.5, belonging to a mixture reaction of two-electron and four-electron.[1] In addition, the Ni_1-B_2@BNC and Ni_7-B_1@BNC exhibit relatively lower H_2O_2 yield of 72.0 and 72.3 mmol h^{-1} g^{-1} and FE_{H2O2} of 54.5% and 73.4% than those of Ni_4-B_1@BNC (128.5 mmol h^{-1} g^{-1} and 94.9%) at 0.6 V_{RHE} (Figures S18 and S19, Supporting Information), indicating that the optimized strain intensity plays an important role in stabilizing the O—O bond to produce H_2O_2 during ORR.

Considering the distinct catalytic activity of Ni-B@BNC nanostructures, XPS studies were initially conducted to decode their electronic structures (**Figure 4**). As can be seen in Figure 4a, the Ni 2p spectra of Ni_1-B_2@BNC, Ni_4-B_1@BNC, Ni_7-B_1@BNC, and Ni@NC show four peaks that can be assigned to the Ni $2p_{3/2}$, Ni $2p_{1/2}$, and two satellite peaks states. The Ni $2p_{3/2}$ and Ni $2p_{1/2}$ states are associated with Ni^{2+}.[26,27] Compared with Ni@NC, the 2p peak position of Ni_4-B_1@BNC is shifted toward the higher energy region, which is attributed to the incorporation of B changing the electronic structure of Ni. The strong interaction between the 2p electrons of B and the 2s electrons of O_2 is beneficial to the preservation of the O—O bond.[28,29] The high resolution N 1s spectra of the Ni_1-B_2@BNC, Ni_4-B_1@BNC, Ni_7-B_1@BNC, Ni@NC, and BNC catalysts in Figure 4b. The N 1s spectrum of Ni_4-B_1@BNC is divided into four peaks at 397.9, 398.8, 400.6, and 401.7 eV, ascribed to N—B, pyridinic-N (N6), pyrrolic-N (N5), and quaternary-N, respectively.[30–32] Ni_4-B_1@BNC possesses the highest N contents in N-B (19.7 at%) and N6 (30.0 at%) species among the five different catalysts, compared to Ni_1-B_2@BNC (17.5 at%, 20.3 at%), Ni_7-B_1@BNC (14.2 at%, 26.5 at%), Ni@NC (0 at%, 20.0 at%), and BNC (19.4 at%, 16.3 at%). The Ni_4-B_1@BNC with optimized strain intensity among the different catalysts is favorable for the formation of the most stable hexagonal boron nitride, which has proved a higher activity and selectivity toward the oxygen reduction to H_2O_2.[7,32] Above all, the Ni_4-B_1@BNC with the optimized strain intensity shows the enhanced adsorption energy for intermediate and stronger ability to stabilize the O—O bond of O_2 during ORR.

DFT calculations were performed to better elucidate the activation mechanism of the Ni_4-B_1@BNC-catalyzed two-electron ORR (**Figure 5**). As shown in Figure S20 in the Supporting Information, the introduction of B significantly increases the length of adjacent Ni—Ni bonds, showing the presence of tensile strain in Ni_4-B_1@BNC. The optimized OOH* binding sites on Ni_4-B_1@BNC, Ni_1-B_2@BNC, and Ni@NC are shown in Figure 5a. The density of states of Ni_4-B_1@BNC, Ni_1-B_2@BNC, and Ni@NC shown in Figure 5b indicate that B changes the state density of Ni-3d orbital near the Fermi level. Compared with Ni_1-B_2@BNC and Ni@NC, the d-band center of Ni_4-B_1@BNC (–1.134 eV) is closer to Fermi level, thereby likely strengthening the adsorption of O_2 and intermediates. Furthermore, the electron localization function analysis revealed that the electrons are more localized around the Ni atoms, suggesting the existence of charge transfer between B and Ni (Figure S21, Supporting Information), thus altered the surface electronic structure that determines the

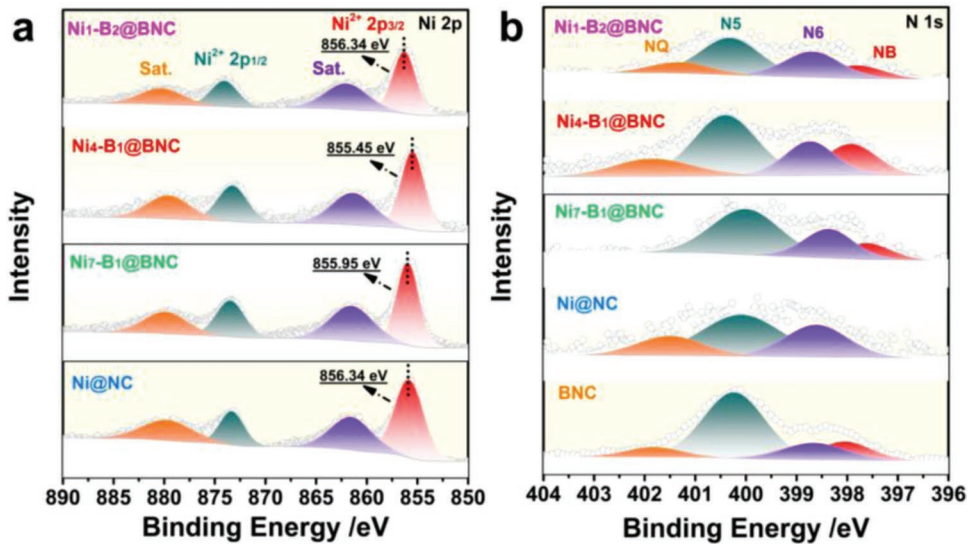

Figure 4. a) Ni 2p spectra and b) N 1s spectra of Ni_1-B_2@BNC, Ni_4-B_1@BNC, Ni_7-B_1@BNC, Ni@NC, and BNC.

ORR activity. Furthermore, Figure 5c shows the free energy of each elementary step under $U = 0$ V and $U = 0.7$ V on Ni_4-B_1@BNC, Ni_1-B_2@BNC, and Ni@NC. For an ideal electrocatalyst toward two-electron ORR, the absolution value of $\Delta G_{(O2\ to\ OOH^*)}$ should be closed to 0, which is propitious to the hydrogenation of O_2 and H_2O_2 production. Among them, Ni_4-B_1@BNC with downhill energy of 0.15 eV to form OOH* exhibits higher catalytic activity than Ni_1-B_2@BNC (1.94 eV) and Ni@NC (1.53 eV). In addition, the overpotential of Ni_4-B_1@BNC, Ni_1-B_2@BNC, and Ni@NC is 0.55, 1.24, and 0.83 V, respectively, revealing that tensile strain introduced by doping B into Ni nanoparticles could optimize the binding energy of OOH* for two-electron ORR.

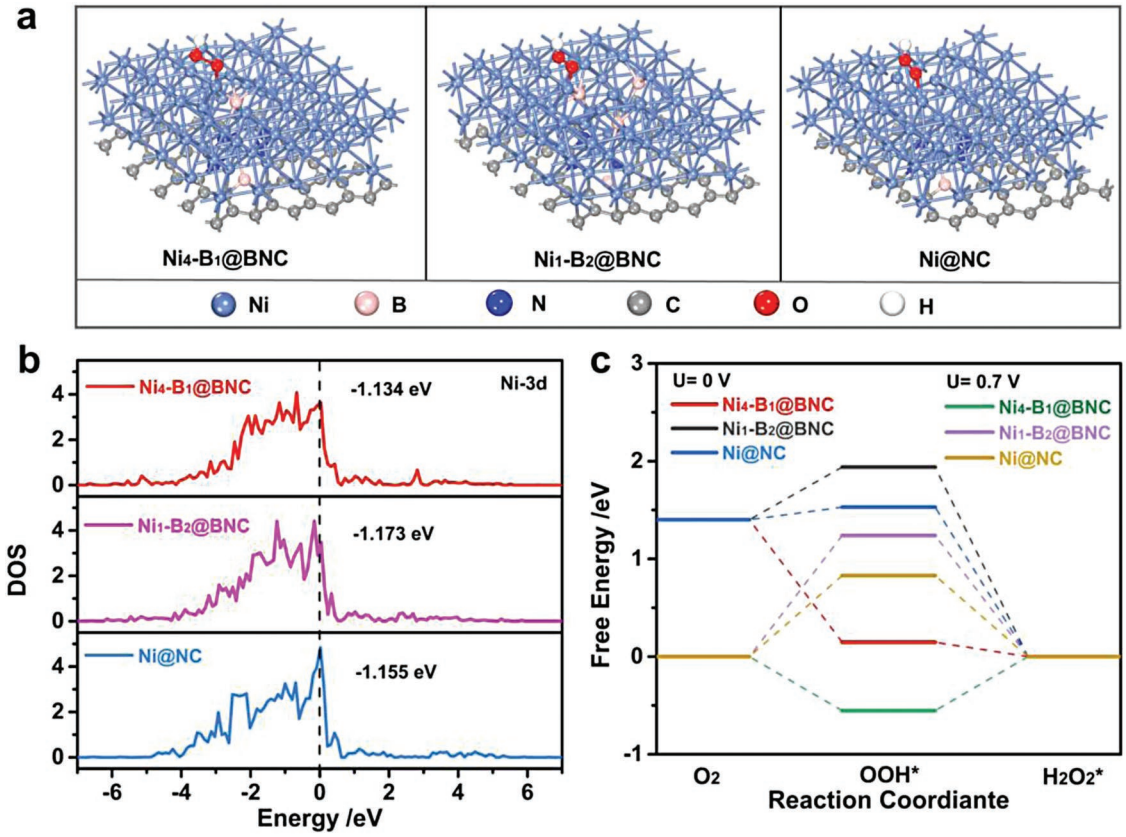

Figure 5. a) Geometry structures of the OOH* adsorption configuration, b) densities of states for Ni-3d, and c) free-energy diagram for oxygen reduction to H_2O_2 of Ni_4-B_1@BNC, Ni_1-B_2@BNC, and Ni@NC.

3. Conclusions

To summarize, Ni-B@BNC composites with tensile strain were synthesized by boronation with $NaBH_4$, which could effectively enhance the adsorption of O_2, stabilize O—O bond and boost the electrocatalytic ORR to H_2O_2. In addition, the tensile strained Ni-B@BNC exhibit volcano-type activity for electrocatalytic ORR to H_2O_2 as a function of the strain intensity, which is controlled by B content. Among them, Ni_4-B_1@BNC exhibits the H_2O_2 selectivity of over 86%, yield of 128.5 mmol h^{-1} g^{-1}, and FE_{H2O2} of 94.9% at 0.6 V_{RHE} toward H_2O_2 production, and excellent long-term stability with 10 h in 0.1 M KOH. DFT calculations reveal that tensile strain introduced by doping B into Ni nanoparticles could decrease the state density of Ni-3d orbital near the Fermi level and optimize the binding energy of OOH* for two-electron ORR. This work provides an avenue for design electrochemical catalysts for two-electron ORR toward H_2O_2 with high performance.

Supporting Information

Supporting Information is available from the Wiley Online Library or from the author.

Acknowledgements

This work was financially supported by the National Natural Science Foundation of China (NSFC) (Grant No. 22105087), Natural Science Foundation of Jiangsu Province (Grant No. BK20210446), and the Fundamental Research Funds for the Central Universities (JUSRP121036). The authors thank the Central Laboratory, School of Chemical and Material Engineering, Jiangnan University.

Conflict of Interest

The authors declare no conflict of interest.

Data Availability Statement

The data that support the findings of this study are available in the supplementary material of this article.

Keywords

boron doping, electrocatalysis, hydrogen peroxide, lattice strain, oxygen reduction reaction

Received: June 6, 2022
Revised: July 12, 2022
Published online:

[1] Y. Jiang, P. Ni, C. Chen, Y. Lu, P. Yang, B. Kong, A. Fisher, X. Wang, *Adv. Energy Mater.* **2018**, *8*, 1801909.
[2] J. Zhang, H. Zhang, M. J. Cheng, Q. Lu, *Small* **2020**, *16*, 1902845.
[3] M. Wang, N. Zhang, Y. Feng, Z. Hu, Q. Shao, X. Huang, *Angew. Chem., Int. Ed.* **2020**, *59*, 14373.
[4] S. Yang, A. Verdaguer-Casadevall, L. Arnarson, L. Silvioli, V. Čolić, R. Frydendal, J. Rossmeisl, I. Chorkendorff, I. E. L. Stephens, *ACS Catal.* **2018**, *8*, 4064.
[5] S. Chen, C. Wang, X. Lu, *Compos. Commun.* **2021**, *27*, 100842.
[6] J. K. Edwards, B. Solsona, E. Ntainjua N, A. F. Carley, A. A. Herzing, C. J. Kiely, G. J. Hutchings, *Science* **2009**, *323*, 1037.
[7] X. Li, X. Wang, G. Xiao, Y. Zhu, *J. Colloid Interface Sci.* **2021**, *602*, 799.
[8] W. P. Mounfield, A. Garg, Y. Shao-Horn, Y. Román-Leshkov, *Chem* **2018**, *4*, 18.
[9] X. Guo, S. Lin, J. Gu, S. Zhang, Z. Chen, S. Huang, *ACS Catal.* **2019**, *9*, 11042.
[10] V. Beermann, M. Gocyla, S. Kühl, E. Padgett, H. Schmies, M. Goerlin, N. Erini, M. Shviro, M. Heggen, R. E. Dunin-Borkowski, D. A. Muller, P. Strasser, *J. Am. Chem. Soc.* **2017**, *139*, 16536.
[11] B. Q. Li, C. X. Zhao, J. N. Liu, Q. Zhang, *Adv. Mater.* **2019**, *31*, 1808173.
[12] Y. Sun, L. Han, P. Strasser, *Chem. Soc. Rev.* **2020**, *49*, 6605.
[13] Z. Lu, G. Chen, S. Siahrostami, Z. Chen, K. Liu, J. Xie, L. Liao, T. Wu, D. Lin, Y. Liu, T. F. Jaramillo, J. K. Nørskov, Y. Cui, *Nat. Catal.* **2018**, *1*, 156.
[14] L. Yang, J. Shui, L. Du, Y. Shao, J. Liu, L. Dai, Z. Hu, *Adv. Mater.* **2019**, *31*, 1804799.
[15] Y. Xiao, J. Hong, X. Wang, T. Chen, T. Hyeon, W. Xu, *J. Am. Chem. Soc.* **2020**, *142*, 13201.
[16] J. Liu, C. Q. Sun, W. Zhu, *Electrochim. Acta* **2018**, *282*, 680.
[17] J. Wang, Z. Huang, W. Liu, C. Chang, H. Tang, Z. Li, W. Chen, C. Jia, T. Yao, S. Wei, Y. Wu, Y. Li, *J. Am. Chem. Soc.* **2017**, *139*, 17281.
[18] Y. Wang, R. Shi, L. Shang, G. I. N. Waterhouse, J. Zhao, Q. Zhang, L. Gu, T. Zhang, *Angew. Chem., Int. Ed.* **2020**, *59*, 13057.
[19] Z. Zhou, Y. Kong, H. Tan, Q. Huang, C. Wang, Z. Pei, H. Wang, Y. Liu, Y. Wang, S. Li, X. Liao, W. Yan, S. Zhao, *Adv. Mater.* **2022**, *34*, 2106541.
[20] L. Zhang, W. Xiao, Y. Zhang, F. Han, X. Yang, *Compos. Commun.* **2021**, *26*, 100792.
[21] W. Li, D. Wang, T. Liu, L. Tao, Y. Zhang, Y. C. Huang, S. Du, C. L. Dong, Z. Kong, Y. F. Li, S. Lu, S. Wang, *Adv. Funct. Mater.* **2022**, *32*, 2109244.
[22] Y. Li, S. Guo, *Nano Today* **2019**, *28*, 100774.
[23] Z. Xia, S. Guo, *Chem. Soc. Rev.* **2019**, *48*, 3265.
[24] Y. Wu, Z. Gao, Y. Feng, Q. Cui, C. Du, C. Yu, L. Liang, W. Zhao, J. Feng, J. Sun, R. Yang, J. Sun, *Appl. Catal., B* **2021**, *298*, 120572.
[25] N. Zhang, F. Zheng, B. Huang, Y. Ji, Q. Shao, Y. Li, X. Xiao, X. Huang, *Adv. Mater.* **2020**, *32*, 1906477.
[26] R. Shen, K. He, A. Zhang, N. Li, Y. H. Ng, P. Zhang, J. Hu, X. Li, *Appl. Catal., B* **2021**, *291*, 120104.
[27] Q. Zhou, Q. Hao, Y. Li, J. Yu, C. Xu, H. Liu, S. Yan, *Nano Energy* **2021**, *89*, 106402.
[28] F. Ma, S. Wang, X. Liang, C. Wang, F. Tong, Z. Wang, P. Wang, Y. Liu, Y. Dai, Z. Zheng, B. Huang, *Appl. Catal., B* **2020**, *279*, 119371.
[29] J. Wu, M. Hou, Z. Chen, W. Hao, X. Pan, H. Yang, W. Cen, Y. Liu, H. Huang, P. W. Menezes, Z. Kang, *Adv. Mater.* **2022**, https://doi.org/10.1002/adma.202202995.
[30] Y. Wen, H. Zhu, J. Hao, S. Lu, W. Zong, F. Lai, P. Ma, W. Dong, T. Liu, M. Du, *Appl. Catal., B* **2021**, *292*, 120144.
[31] Y. Wen, Z. Zhuang, H. Zhu, J. Hao, K. Chu, F. Lai, W. Zong, C. Wang, P. Ma, W. Dong, S. Lu, T. Liu, M. Du, *Adv. Energy Mater.* **2021**, *11*, 2102138.
[32] S. Chen, Z. Chen, S. Siahrostami, D. Higgins, D. Nordlund, D. Sokaras, T. R. Kim, Y. Liu, X. Yan, E. Nilsson, R. Sinclair, J. K. Nørskov, T. F. Jaramillo, Z. Bao, *J. Am. Chem. Soc.* **2018**, *140*, 7851.